The Iron Abundance and Density Structure of the Inner Ring Around SN 1987A

S.Mattila[1], P.Lundqvist[1], P.Meikle[2], R.Stathakis[3], and R.Cannon[3]

[1] Stockholm Observatory, AlbaNova, Dept. of Astronomy, Stockholm SE-106 91, Sweden seppo@astro.su.se
[2] Blackett Laboratory, Imperial College, Prince Consort Road, London SW7 2BW, UK
[3] Anglo-Australian Observatory, PO Box 296, Epping, NSW 1710, Australia

Summary. We present a spectroscopic study of the inner circumstellar ring around SN 1987A. The aim is to determine the elemental abundances and density structure, with particular emphasis on the abundance of iron. We acquired and analyzed optical spectra at the Anglo-Australian Telescope (AAT) between 1400 and 4300 days post-explosion. We also assembled from the literature all available optical/near-IR line fluxes of the inner ring. The observed line light curves were then compared with a photoionization model for the inner ring. This indicates an iron abundance of $(0.20\pm0.08) \times$ solar which is lower than that generally seen in the Large Magellanic Cloud (LMC).

1 Motivation

X-ray observations [2] indicate an iron abundance of $0.1 \times$ solar for the circumstellar medium (CSM) of SN 1987A. This is surprisingly low compared to the iron abundances, ranging between $\sim$0.25 and $\sim$0.50 $\times$ solar, e.g. [7,9,1], generally observed in the LMC. Such a large under-abundance of iron could result from the depletion of iron on dust grains in the red supergiant wind of the progenitor star before the supernova (SN) exploded.

2 The Observed Line Light curves for the Inner Ring

2.1 AAT Observations of SN 1987A Inner Ring

Optical spectroscopic observations of SN 1987A were carried out using the Royal Greenwich Observatory (RGO) Spectrograph on the AAT between 1991 and 1998. Data were obtained at four different epochs: 1416, 1680, 1991, and 4309 days post-explosion. At each epoch, the observations comprised a brief, wide slit integration (5-15 min; 5.3"-10.0"), and a longer duration, narrow slit integration (1-3 hours; 1.5”-2.0”). The SN observations spanned air masses ∼1.5 to ∼3.0 (i.e. zenith distances of 50 to 70 degrees), making accurate flux calibration quite challenging. We therefore carried out the observations with the slit position angle (PA) set to be roughly the same as the line joining Stars 2 and 3. This meant that Star 2 lay well within the broad slit and so could be used to correct for the variable transmission of the atmosphere (for details see [14]). However, an additional problem was that, since the slit PA was generally not at the parallactic angle, when the narrow slit was used, atmospheric refraction could introduce wavelength-dependent vignetting of the ring spectra. Moreover, the magnitude of this effect differed from that experienced by Star 2 since the latter lay nearer the edge of the slit. Consequently, the flux uncertainty introduced could be as large as ±40%.

2.2 Star 3 Contamination Removal Using HST Archival Data

The AAT observations suffered from seeing ranging between ∼1” and ∼3” and so the inner ring spectra were always significantly contaminated by light from the two nearby stars. In general, the CSM emission lines could be easily distinguished from the continuum originating from the SN and the two stars. However, Star 3 is a Be star showing strong Hα and Hβ emission together with optical variability of ∼0.5 magnitudes [22]. Consequently, it could affect significantly the observed line fluxes from the inner ring, especially at the later epochs when the ring was fainter. To assess and correct for possible Star 3 contamination, we searched the HST archive for suitable optical spectroscopic (STIS) and photometric (WFPC2) observations.

STIS spectra with a large enough slit aperture (52”x2”) and suitable centering and orientation to include Star 3 were selected from the HST archive. These spectra confirm the findings of Wang et al. [22] that there are indeed no forbidden lines present in the Star 3 spectrum (see [14]). The vignetted narrow slit spectra were therefore scaled in flux to match those of the unvignetted broad slit spectra using the brightest forbidden lines present in both the spectra. Deriving line fluxes for the whole inner ring this way assumes homogeneous ring geometry. WFPC2 F502N and F656N images which were contemporary with our AAT spectra were then selected from the HST archive. Average Hα and Hβ fluxes of 44 and 13 $\times$ 10^{-15} erg s^{-1} cm^{-2}, respectively, were found for Star 3, with a maximum variability of ∼20% over a 6 year time span. These fluxes were used to correct for Star 3 contamination of the hydrogen line fluxes in the broad slit AAT observations. In addition, the accuracy of the absolute flux of our AAT observations was checked using the HST inner ring data. This indicates that our ground-based fluxes are consistent with the HST measurements to within the estimated errors of ±20-40%.

2.3 The Line Light Curves

From the AAT spectra, we measured optical line fluxes at 1416, 1680, 2864 and 4309 days for H, He, N, O, Ne, S, Ar, Ca and Fe (e.g. Fig.1). We also assembled from the literature all available optical/near-IR line fluxes of the inner ring. This includes data from the following sources: [19] (307 days), [20] (511, 552, 586, 678, and 735 days), [15] (574, 668, 695, 734, 840, 958, and 1114 days), [16] (1050 days), [21] (1280 days), [3] (1344 days), [5] (1348, 1469, 1734, 1822, and 2122 days). The resulting dataset (see [14]) spans $300 - 4300$ days post-explosion, i.e., from the time when the ring first became visible to the time when the first signs of ejecta/ring collision were seen at these wavelengths.

2.4 Modeling the Line Light Curves of the Inner Ring

The latest version of the photoionization code described in [10, 11, 12] was used to model the emission line light curves of the inner ring. In the model the ring is initially ionized by the soft X-ray and UV photons emitted in the SN shock break-out. The SN flash with the temporal and spectral characteristics of the 500full1 model [4] sets up the initial ionization structure of the ring, and the gas then recombines and cools. To model the emission line fluxes of iron, we collected from the literature the latest atomic data for the most abundant ions of iron in the ring (see [14]). Thanks to the Iron Project [8] these atomic data have improved significantly during the last few years and now make such abundance determinations more reliable.

2.5 The Density Structure

The mass and density structure of the ionized gas in the inner ring was determined by searching for satisfactory model fits for (1) the absolute line fluxes of Hα and Hβ (Fig.1A-B), and (2) the observed time evolution of the line fluxes of all the other elements (e.g., Fig.1C-D). We found that five density components were needed: 10^3, 2×10^3, 3×10^3, 2×10^4, and 4×10^4 atoms cm^{-3} with masses of ionized gas of 0.4, 1.1, 1.0, 0.8, and 0.5×10^{-2} M$_{\odot}$, respectively. The low-density components dominate the line light curves at the later times. High resolution (HST) images indicate that this low-density gas is situated, on average, further away from the SN than the gas with a higher density [13]. In reality there is also probably a continuous range of densities within the ring rather than a few discrete density components.

2.6 The Iron Abundance

The elemental abundances yielding the observed absolute line fluxes were then determined (Fig.1E-J). This was done by altering the total number of emitting ions relative to hydrogen. However, we have not yet included the effects of these modified abundances on the temperature and ionization structure of the ring. Therefore, the abundances derived for the more abundant elements, e.g. He, N, O, should be considered as only preliminary results (e.g. Fig.1C-D).

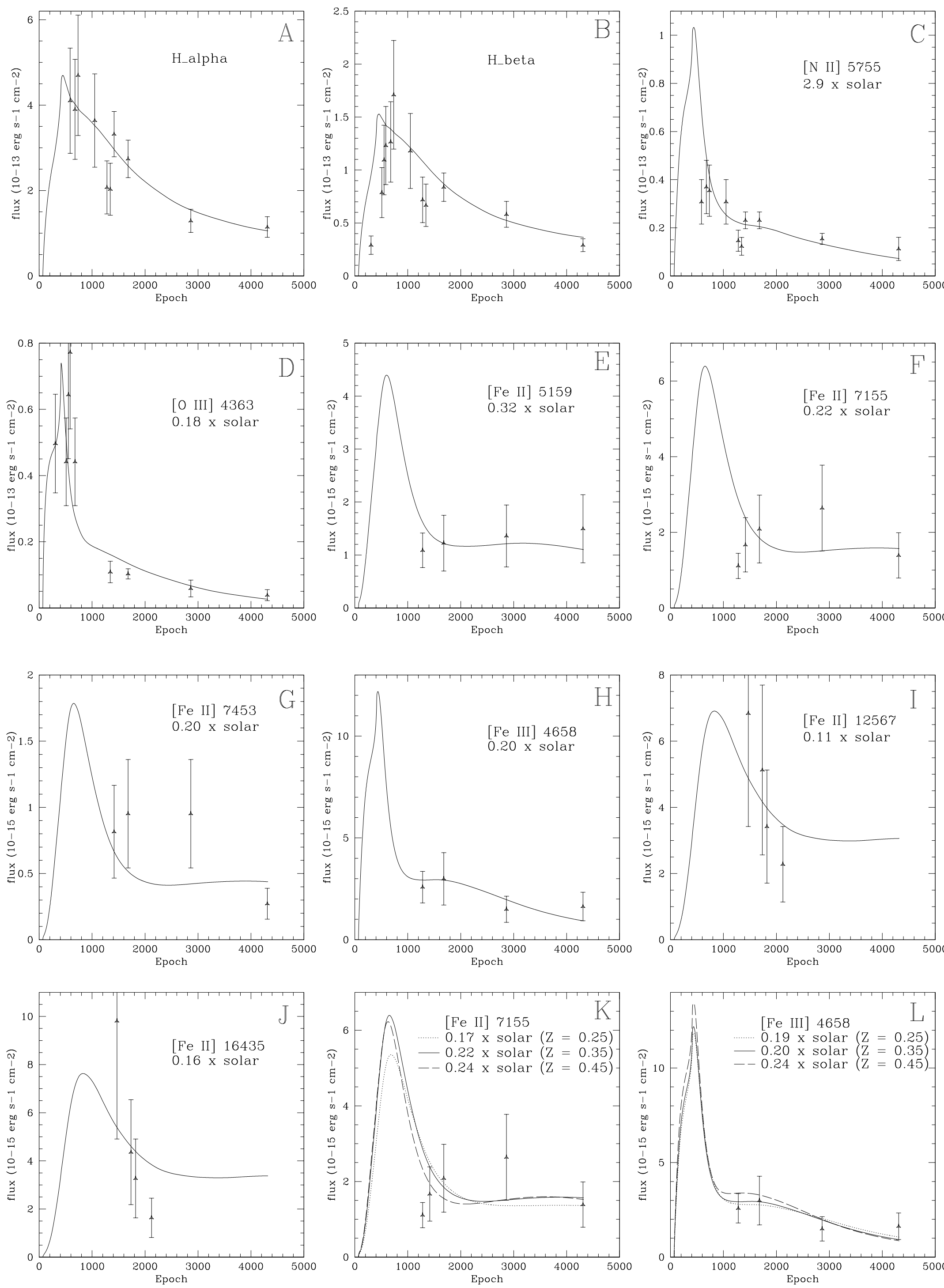

Fig. 1. A − J : The observed fluxes of lines of H, N, O, and Fe plotted together with the model fluxes. The observed line fluxes have been dereddened assuming E_{B-V} of 0.05 and 0.15 for the Galaxy and the LMC, respectively. The abundance used for each model fit is given relative to solar. **K − L** : The observed line fluxes of [Fe II] 7155Å and [Fe III] 4658Å plotted together with the model fluxes for three different metallicities.

However, the effect of the modified iron abundance on the temperature and ionization structure is not significant, thus allowing its robust determination.

Our estimate of the iron abundance is based on five [Fe II] and one [Fe III] lines (Fig.1E-J). This indicates an average abundance of 0.20 times solar with a dispersion of 35%. In addition, we estimated the effects of the assumed He, N, and O abundances and the overall metallicity on the determined iron abundance. We found that the iron model fluxes are rather insensitive to the He/H and N/O ratios. However, the overall metallicity has a much larger effect on the cooling, and thus on the iron model line light curves (Fig.1K-L). We estimate that this introduces an uncertainty of 15% in the average iron abundance. Therefore, from this study, we deduce an iron abundance of (0.20 ± 0.08) times solar (see [14]). This abundance is larger by a factor of two relative to that found by Borkowski, Blondin & McCray [2] from X-ray observations. However, it is at the lower end of the iron abundance range (0.25-0.50 times solar) found for different locations within the LMC. We note that also an inner ring silicon abundance of a factor of $\sim$2 lower than normal for the LMC was found recently by Lundqvist & Sonneborn [13]. These low abundances are probably due to depletion onto dust grains. The existence of dust in the ring material has been demonstrated by mid-IR observations [17, 6].

Acknowledgement. We thank L. Smith, R. Terlevich, and R. Cumming for helpful discussions.

References

1. Andrievsky S.M. et al.: A&A **367**, 605 (2001)
2. Borkowski K.J., Blondin J.M., McCray R.: ApJL **476**, L31 (1997)
3. Cumming R.: PhD Thesis, Imperial College, University of London (1994)
4. Ensman L. & Burrows A.: ApJ **393**, 742 (1992)
5. Fassia A., Meikle W.P.S., Spyromilio J.: MNRAS **332**, 296 (2002)
6. Fischera J., Tuffs R.J., & Völk H. J.: A&A **386**, 517 (2002)
7. Hughes J.P., Hayashi I., Koyama K.: ApJ **505**, 732 (1998)
8. Hummer D.G. et al: A&A **279**, 298 (1993)
9. Korn A.J., Becker S.R., Gummersbach C.A., Wolf B.: A&A **353**, 655 (2000)
10. Lundqvist P. & Fransson C.: ApJ **380**, 575 (1991)
11. Lundqvist P.: PASP **104**, 787 (1992)
12. Lundqvist P. & Fransson C.: ApJ **464**, 924 (1996)
13. Lundqvist P. & Sonneborn G.: SN 1987A: Ten Years After, Workshop (2004)
14. Mattila S.: PhD Thesis, Imperial College, University of London (2002)
15. Meikle W.P.S. et al: MNRAS **261**, 535 (1993)
16. Menzies J.W: SN 1987A and other SNe, ESO/EIPC Workshop, 209 (1991)
17. Roche P.F. et al: Nature **337**, 533 (1989)
18. Scuderi S. et al: ApJ **465**, 956 (1996)
19. Wampler E.J. & Richichi A.: A&A **217**, 31 (1989)

20. Wampler E.J. et al: IAU Colloq. 120, 180 (1989)
21. Wang L.: A&A **246**, L69 (1991)
22. Wang L. et al: IAUC, 5449 (1992)